Membrane deflection in a flat membrane microcontactor : experimental study of spacer features

Membrane deflection in a flat membrane microcontactor: experimental study of spacer features

Jonas Hereijgers[a,c], Heidi Ottevaere[b], Tom Breugelmans[c] and Wim De Malsche[a*]

[a]*Department of Chemical Engineering, Vrije Universiteit Brussel, Pleinlaan 2, 1050 Brussel, Belgium*

[b]*Brussels Photonics Team (B-PHOT), Department of Applied Physics and Photonics, Vrije Universiteit Brussel, Pleinlaan 2, 1050 Brussel, Belgium*

[c]*Faculty of Applied Engineering, Research group Advanced Reactor Technology, University of Antwerp, Salesianenlaan 90, 2660 Hoboken, Belgium*

*Corresponding author: tel. (+) 32/ 2.629.33.18, fax (+) 32/ 2.629.32.48, e-mail:

wdemalsc@vub.ac.be

Graphical abstract

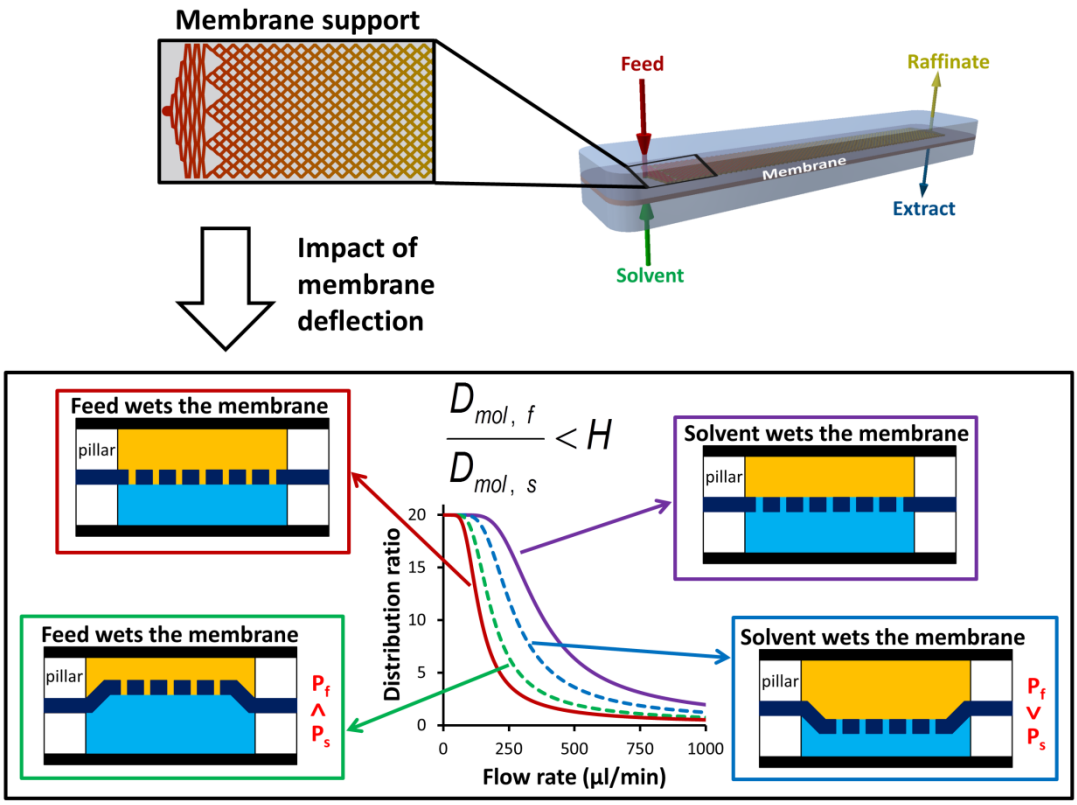

Abstract

In this work, the impact of the spacer features (interpillar distance and shape) on the membrane deflection, pressure difference across the membrane, and mass transfer was studied for a flat membrane microcontactor. It was demonstrated that decreasing the interpillar distance between the circular pillars reduced membrane deflection considerably. As a consequence, also the pressure difference across the membrane decreased, which lowers the possibility of breakthrough occurring. However, this was only the case until an interpillar distance of 836 µm was reached. Decreasing the interpillar distance further, the pressure difference across the membrane again increased. This was due to the smaller gap between the pillars, resulting in a higher hydraulic resistance. However, it was demonstrated that with the use of a channel filled with radially elongated (diamond shaped) pillars

and wedges the pressure difference across the membrane remained minimal at small interpillar distances (i.e. 305 µm). Finally, the effect of the membrane deflection on the mass transfer was studied. It was shown that membrane deflection can have either a positive or negative impact on the mass transfer and solvent inside the pores instead of the feed is not always beneficial when membrane deflection is taken into account. Therefore, design rules for the spacer geometry are deduced, which allows maximizing mass transport.

Keywords

solvent extraction; membrane contactor; spacer; membrane deflection; support features

List of Symbols

AR	aspect ratio	(\)
CP	circular pillar	(\)
C	concentration	(mol/m³)
D	molecular diffusion coefficient	(m²/s)
d_{fiber}	fiber diameter	(m)
d_{pore}	pore diameter	(m)
h	channel height	(m)
H	partition coefficient	(\)
k	local mass transfer coefficient	(m/s)
K	global mass transfer coefficient	(m/s)
L	channel length of the MMC	(m)
L_{fiber}	fiber length	(m)
MMC	membrane microcontactor	(\)

REP	radially elongated pillar	(\)
Sh	Sherwood number	(\)
SX	Solvent extraction	(\)
u	velocity	(m/s)
$\Delta h_{m,\,max}$	average maximal membrane deflection height	(m)
ΔP_{axial}	axial pressure drop	(bar)
$\Delta P_{m,\,max}$	average maximal pressure difference across the membrane	(bar)
$\Delta P_{m,\,min}$	average minimal pressure difference across the membrane	(bar)

Greek letters:

δ	membrane thickness	(m)
ε	membrane porosity	(%)
τ	membrane tortuosity	(\)

Subscripts:

f	feed
m	membrane
s	solvent
tot	total

1 Introduction

Membrane contactors are interesting tools for solvent extraction (SX). In SX operations coalescence in the phase separation step is usually of prime importance, as it dictates the overall throughput [1]. By placing a membrane at the interface between two immiscible liquids, the interface is stabilized [2] and the phase separation step can be omitted.

Two types of membrane contactor configurations exist: the flat sheet configuration, which can also be spiral wounded to minimize space and the hollow fiber (or tubular) configuration [2], [3]. Of these two configurations, the hollow fiber is often the preferred configuration, because of their large specific surface (500-5000 m^2/m^3 [4]). Flat sheet membrane contactors typically have a limited specific surface ranging from 100 to 2000 m^2/m^3 [5]. The hollow fiber approach, however, has some disadvantages: harder to fabricate then flat sheet membranes (e.g. mechanical stability) [3]; multiple fibers packed in one module leads to shell side maldistribution [2]; irreversible sealing; potting adhesive prone to solvent attacks.

Increasing the specific surface for the flat sheet membrane approach would, consequently, be well perceived by the academic community and industry. The problem, however, with flat sheet membranes is that they need to be supported and these supports are typically a few hundred micrometers thick, resulting in limited specific surface and consequently in slow mass transfer kinetics.

Using microfabrication technology we constructed so-called membrane microcontactors (MMCs) with spacers thicknesses in the range of 200 to 50 µm, resulting in high specific surfaces of 5000 to 20000 m^2/m^3 [5], [6]. Doing so, extraction rate was high and equilibrium could be obtained in a matter of minutes.

Crucial when using membrane microcontactors, is the stability of the liquid-liquid interface so that a phase separation step can be avoided. When the pressure difference across the membrane (ΔP_m = $P_{non\text{-}wetting\ phase} - P_{wetting\ phase}$) is larger than the breakthrough pressure, the non-wetting phase will displace the wetting phase inside the pores of the membrane and the non-wetting phase disperse in the wetting phase channel (Fig. 1). Also, when the pressure of the wetting phase is larger than the pressure of the non-wetting phase, breakthrough occurs, because the wetting phase will disperse in the non-wetting phase, as the membrane will no longer hold the wetting phase back. Consequently, to avoid breakthrough, a pressure difference across the membrane is needed with the non-wetting phase at a higher pressure than the non-wetting phase, but so that ΔP_m is below the breakthrough pressure. This critical breakthough pressure is determined by the membrane characteristics (i.e pore size and shape) and the liquid properties (i.e. interfacial tension and contact angle). Different models exist to describe the breakthrough pressure, of which the validity has been studied in previous work [7].

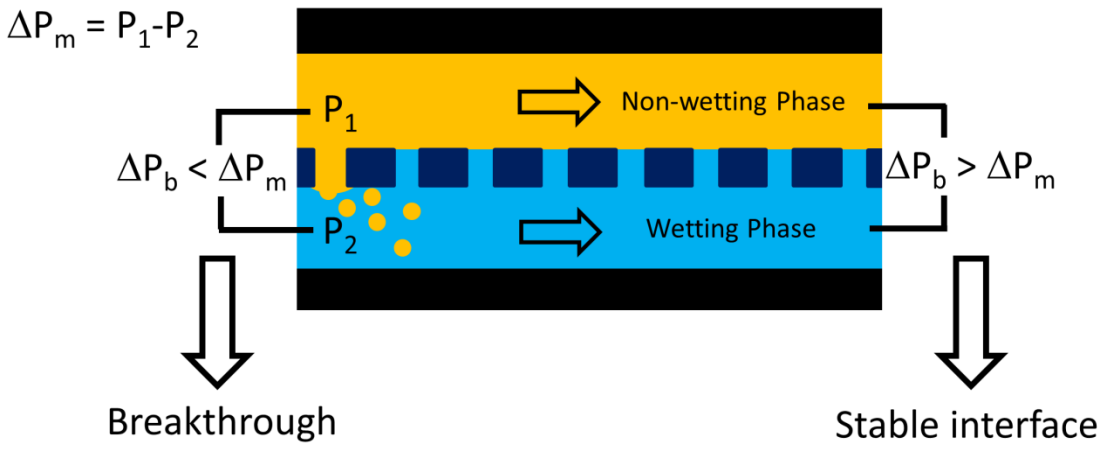

Fig. 1: Schematic representation of breakthrough. ΔPb = breakthrough pressure

Because a pressure difference across the membrane is necessary to obtain a stable interface, the membrane can deflect (Fig. 2). When the membrane deflects, the channel depth of the feed (h_f) and solvent (h_s) will alter. As a consequence, this will influence ΔP_m and the extraction rate.

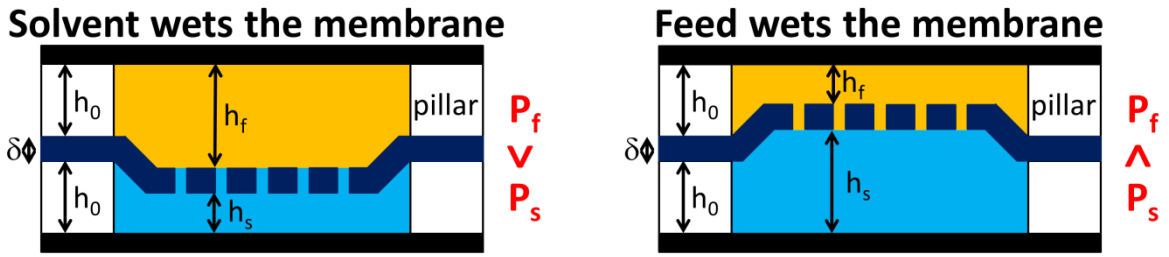

Fig. 2: Schematic representation of the membrane deflection for solvent and feed wetting the membrane.

When there is no membrane deflection and the viscosity of the non-wetting phase is larger than the wetting phase, the pressure profile inside the MMC resembles to Fig. 3a (solid lines). As at the inlet and outlet there is still a difference in pressure between the wetting and non-wetting phase, ΔP_m can be decreased by increasing the backpressure (dotted line). This will raise the pressure inside the wetting phase channel and decrease $\Delta P_{m,\,max}$ and consequently throughput can be higher before breakthrough occurs. When there is bending of the membrane (Fig. 3b), the axial pressure drop inside the wetting phase channel will be larger (steeper decline of the blue solid line), due to a smaller channel height. Consequently, $\Delta P_{m,\,max}$ is larger for a similar throughput and is now located at the inlet.

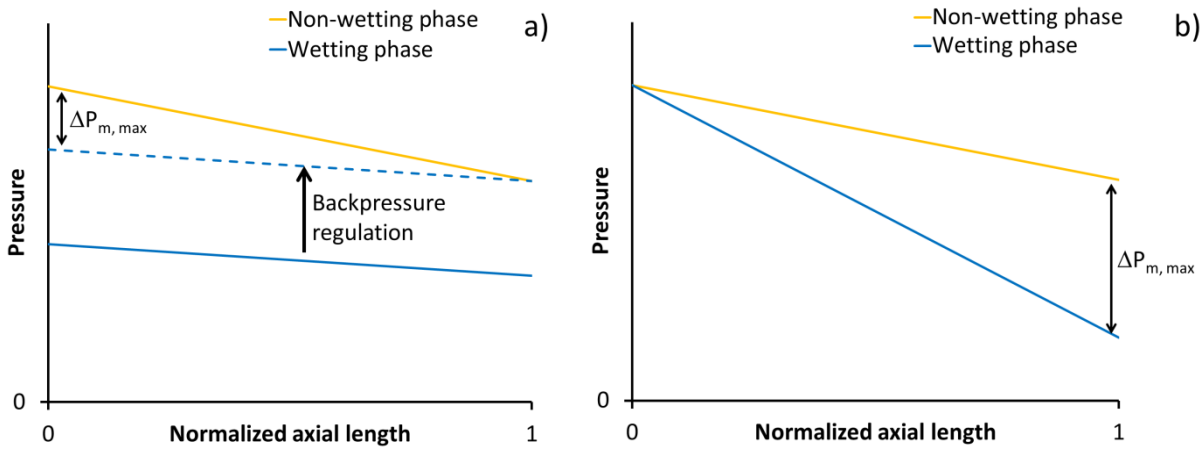

Fig. 3: Schematic representation of the pressure profile inside the MMC as function of the normalized axial length (x/L): a) without membrane deflection; b) with membrane deflection.

Because the channel heights will alter due to deflection of the membrane (Fig. 2), the path the solute has to diffuse from feed to extraction solvent will vary and this will consequently also influence the extraction rate.

As with MMCs the channels are much thinner than with traditional membrane contactors, to increase extraction rate, the impact of membrane deflection will be much more pronounced. Consequently, the spacer geometry (i.e. pillar spacing and shape) should be optimized. In this work the impact of the support structure on the deflection of the membrane, pressure difference across the membrane, and concomitantly mass transfer in MMCs is investigated. From these results design guidelines for the spacer geometry are deduced, which allow to derive case specific design requirements.

2 Experimental

2.1 Chemicals

n-Heptane and methyl isobutyl keton (MIBK) were purchased from Acros Organics with a purity of 99+%. The water used throughout the experiments was prepared in the laboratory (Milli-Q-gradient, Millipore, Bedford, MA, USA).

2.2 Membrane microcontactor

The MMC (Fig. 4) consisted of two polyoxymethylene (POM) bodies, which clamp the membrane (Fig. 4, Table 1). Inside the POM bodies, using a micro-precision mill (Datron M7 CNC mill), a channel with spacer features of 100 µm deep, 13 mm wide and 99 mm long was milled (Fig. 8), with a milling error of 10 µm. Using this tool, different sets of POM bodies were made with different spacer geometry (Table 2). Before clamping, the membrane was stretched around the POM body to avoid rippling and a Kalrez o-ring (Eriks, Belgium) was placed around the channel to ensure sealing upon

clamping. An aluminum holder was placed around the POM bodies and tightened with bolts in stages from 1 Nm to 2.5 Nm, 5 Nm and finally 7.5 Nm using a torque wrench to guarantee a uniform clamping strength.

Table 1: Properties of the used membranes.

Membrane	**material**	**pore size**	**thickness**	**porosity**
Advantec T010A293D	PTFE	100 nm	70 µm	68 %
Celgard 2500	polypropylene	64 nm	25 µm	55 %

Table 2: Specification of the studied pillar arrays (CP = circular pillar; REP = radially elongated pillar; AR = aspect ratio (length/width)).

	Pillar shape	Interpillar distance (µm)
1	CP	3000
2	CP	1333
3	CP	836
4	CP	400
5	CP	305
6	REP (AR 1)	305

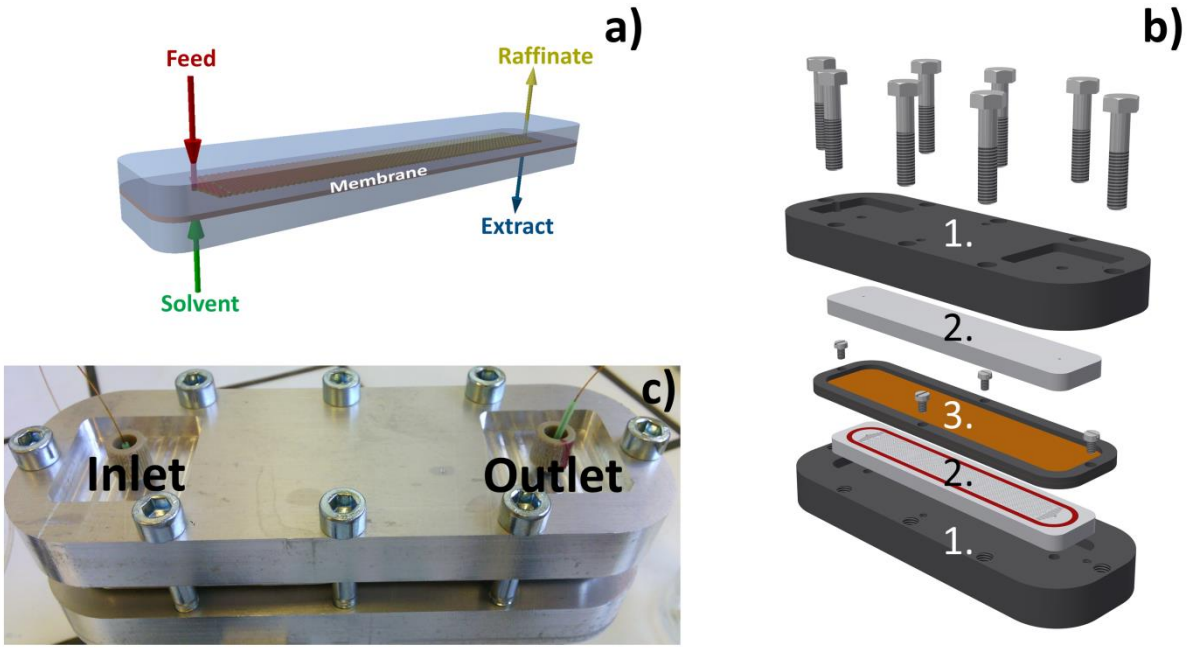

Fig. 4: a) Schematic representation of the MMC, b) exploded view of the MMC (1. aluminum holder; 2. POM body; 3. membrane stretched onto an aluminum ring) and c) picture of the fully assembled MMC.

2.3 Constant pressure operation

Under constant pressure operation the feed and solvent flows to the MMC are provided by two pressure vessels, which allows operating under constant pressure mode. These two vessels were filled with water and n-heptane and the bottom of the vessels were connected to the MMC. The top of each vessel was connected to the same pressure regulator, guaranteeing an identical pressure inside each vessel. Pressurized air was used to regulate the pressure. The accompanying flow rate was gravimetrically determined by collecting each phase at the outlet. Each sample was also visually checked, to guarantee a breakthrough free operation.

2.4 Membrane deflection

The membrane deflection was measured for different spacer designs (Table 2) and two different membranes (Advantec T010A304D and Celgard 2500). To measure the membrane deflection, a white-light interferometer was used (Bruker GT-I). However, to allow for measuring the membrane deflection with an interferometer, the membrane must be exposed, as the incoming light has to

reflect directly onto the membrane surface (Fig. 5a). To this end, the MMC holder was adjusted (Fig. 5b-c). The holder now only contains one POM body around which the membrane is stretched. At the front side of the holder a viewing window is foreseen, leaving the membrane exposed. However, if the pressure beneath the membrane is larger than the atmospheric pressure, the membrane would deflect away from the POM body, preventing measuring the impact of the spacer design on the membrane deflection. To this end, the membrane must be pulled inwards. To do this, a syringe pump (WPI Aladdin-1000) in the withdraw mode was used, such that the pressure beneath the membrane was lower than atmospheric pressure. Due to this withdraw mode, n-heptane was sucked from the reservoir through the channel towards the syringe and the membrane was pressed into the channel. To avoid air being sucked through the pores of the membrane, n-heptane was used, as the tested membranes (Advantec T010A304D and Celgard 2500) are hydrophobic. If for instance water would be used, the pores would be filled with air, and there would be no capillary action holding the air back. In that case, the pressure beneath the membrane would be almost equal to the atmospheric pressure, as air is continuously sucked through the pores and consequently no membrane deflection was observed.

The deflection of the membrane was always measured at the center of the channel, using an automated translation table and the axial pressure drop across the MMC channel was measured by two pressure sensors (Gefran, model no. TK-N-1-E-N01U-M-V) positioned at the inlet and outlet (Fig. 5a). By varying the withdraw speed of the syringe pump, the axial pressure drop was regulated.

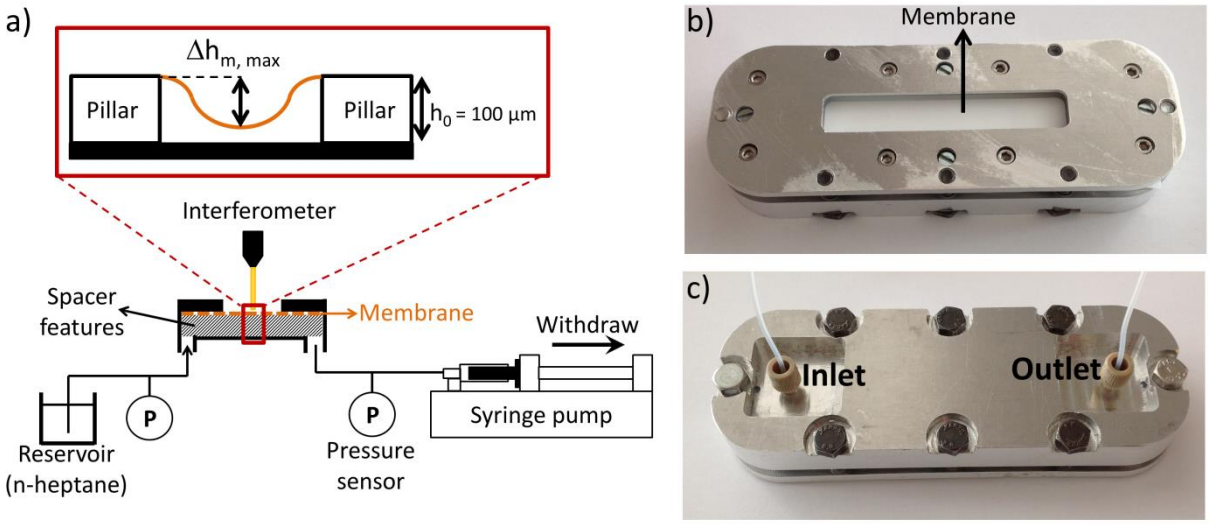

Fig. 5: a) Schematic representation of the interferometer set-up. Picture of the b) front and c) back of the assembled holder for the interferometer set-up.

The data from the interferometer was analyzed with the accompanying Vision64 software, which allows for stitching multiple images. Subsequently, this data was imported into Matlab R2014b to calculate the averaged maximum deflection height of the membrane ($\Delta h_{m,\,max}$) (see supporting information).

2.5 Pressure drop

The maximum pressure difference across the membrane ($\Delta P_{m,\,max}$) was determined for different flow rates, the two membranes (Advantec T010A304D, Celgard 2500) and the different spacer features, using the MMC assembly depicted in Fig. 4b. To measure the pressure difference, pressure sensors (Gefran, model no. TK-N-1-E-B01D-H-V) were placed at the inlets and outlets of the MMC (Fig. 6). The n-heptane and water flows were provided by two HPLC pumps (Shimadzu, LC10-AD) in constant flow mode. The pressure of water and n-heptane at the outlet was regulated using two backpressure regulators (Vici JR-BRP1).

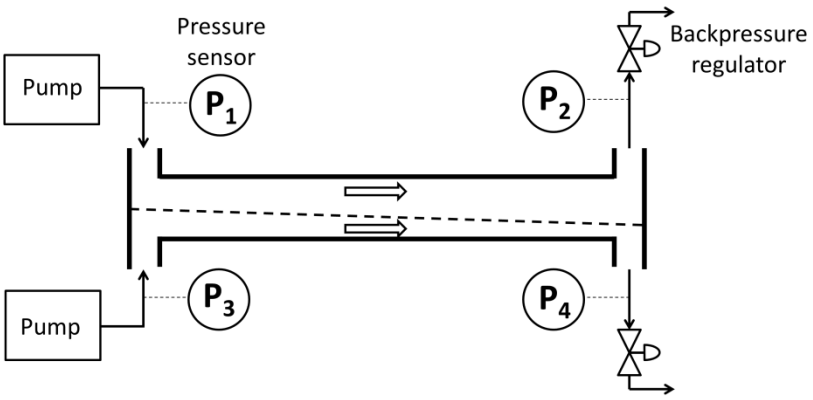

Fig. 6: Set-up to measure the pressure difference across the membrane in function of the flow rate.

3 Results

3.1 Spacer designs

Proof of the membrane deflection can be obtained by flowing two immiscible liquids in constant pressure mode through the MMC. In this case, the flow rate ratio is expected to be constant and independent of the applied pressure. Using a MMC with circular pillars (CP) spaced far apart (3000 µm) it was clear that the flow rate ratio was not constant (Fig. 7), indicating that axial pressure drop is not only function of the velocity. If the membrane deflects, the height of the channel varies with the applied pressure.

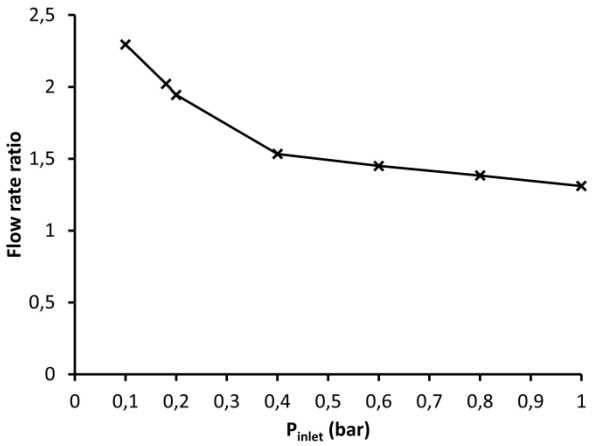

Fig. 7: Flow rate ratio (MIBK/water) in function of the inlet pressure under constant pressure mode for a MMC with CPs spaced 3000 µm apart and equipped with the Advantec T010A304D membrane.

Therefore, a spacer is required, but it should fulfill the following constraints: (1) the pressure difference across the membrane should be lower than the breakthrough pressure and (2) a negative impact on the extraction rate should be avoided.

If the membrane deflection is large, the channel height will be strongly reduced (Fig. 6) and due to this the axial pressure drop will increase ($P_3 >> P_4$). However, at the other side of the membrane the channel height will subsequently increase, which will decrease the axial pressure drop in that channel ($P_1 \approx P_2$). Because of this combined effect the pressure difference across the membrane (P_2-P_4) will increase, which can potentially lead to breakthrough. By placing spacer features inside the channel, this membrane deflection can be reduced. However, if the spacing between these features is small, the axial pressure drop and pressure difference across the membrane will again increase, this time due to the spacer itself. For example, if the spacing between the support structures would be zero, there would be no membrane deflection, but the axial pressure drop would be infinite. Hence, an optimal spacer design is required, keeping on the one hand membrane deflection minimal and on the other hand keeping the pressure difference across the membrane below the breakthrough pressure.

To support a flat membrane usually a porous frit is used, which is however not suited to function as a spacer because of its excessive thickness (in practice in the range of millimeters). Alternatively, the channel could be filled with beads to support the membrane. This approach, however, involves the following drawbacks: (1) some sort of fixation of the beads is required, to prevent flushing-out; (2) packing the channel regularly with the beads is near to impossible to achieve. Because of the irregular packing, channeling effects will arise with a negative impact on the mass transfer and pressure drop, potentially leading to breakthrough. In contrast, no channeling and minimal pressure drop is achieved with regularly structured packings [8]. Therefore, regular pillar arrays are most suited as spacer structures (Fig. 8).

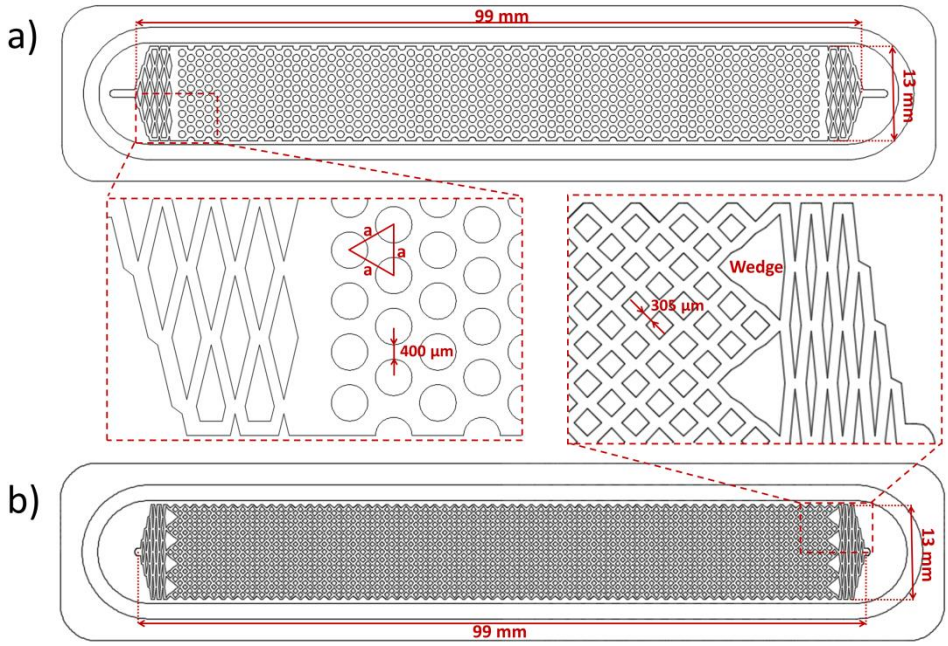

Fig. 8: a) MMC channel filled with circular pillar (CP) spacer features spaced 400 µm apart in an equilateral pattern. b) MMC channel filled with radially elongated pillar (REP) spacer features spaced 305 µm apart.

The channel of the MMC consists of two parts: (1) distributor features at the inlet and outlet and (2) a pillar array to support the membrane. To increase the throughput a relatively large channel width was chosen, i.e. 13 mm. Because the channel is now much wider than the inlet and outlet through-hole (1 mm), radially elongated pillars (REP) had to be placed near the entrance and the outlet of the channel to distribute the liquid evenly and to minimize entrance effects [6]. Wedges were used to make the transition between the distribution REPs with an aspect ratio (AR) of 10 (=width/length) and the REPs with an AR of 1 (Fig. 8b). By lowering the AR, the porosity of the bed increases, which lowers the axial pressure drop. The different pillar array designs examined in the following sections are given in Table 2.

3.2 Impact of the spacer design on the membrane deflection

Looking at Fig. 9 it is clear that $\Delta h_{m,\,max}$ strongly varies with ΔP_{axial} and the spacer design (see supporting information §S.1 for the determination of $\Delta h_{m,\,max}$). Decreasing the pillar distance reduces

$\Delta h_{m,\,max}$ considerably. For the Celgard 2500 membrane complete deflection (channel depth: 100 ± 10 µm) was obtained at ΔP_{axial} = -0.55 bar when the circular pillars were placed 1333 µm apart. By decreasing the interpillar spacing to 305 µm, $\Delta h_{m,\,max}$ was decreased to 18.3 µm at a ΔP_{axial} of -0.58 bar. When the circular pillars were spaced 3000 µm apart, also the Advantec T010A304D membrane was pressed to the bottom of the channel. Also the membrane itself influences $\Delta h_{m,\,max}$. Thinner and more porous membranes are interesting because they yield a lower mass transfer resistance, but they will also have a lower mechanical strength, resulting in a larger deflection and concomitantly in a larger $\Delta h_{m,\,max}$. This is seen with the Advantec T010A304D and Celgard 2500 membrane. With a CP spacer with an interpillar distance of 836 µm and the Advantec T010A304D membrane, $\Delta h_{m,\,max}$ was 46.7 µm with an axial pressure drop of 0.60 bar whereas for the Celgard 2500 membrane which is 45 µm thinner, $\Delta h_{m,\,max}$ was 77.3 µm at an axial pressure drop of 0.52 bar. Hence, thinner and more porous membranes will require a smaller interpillar distance to keep the membrane deflection acceptable. Changing the spacer geometry from CPs to REPs with the same interpillar distance (305µm) did not alter the membrane deflection; it remained small for both membranes; beneath 10 µm for a ΔP_{axial} lower than 0.35 bar.

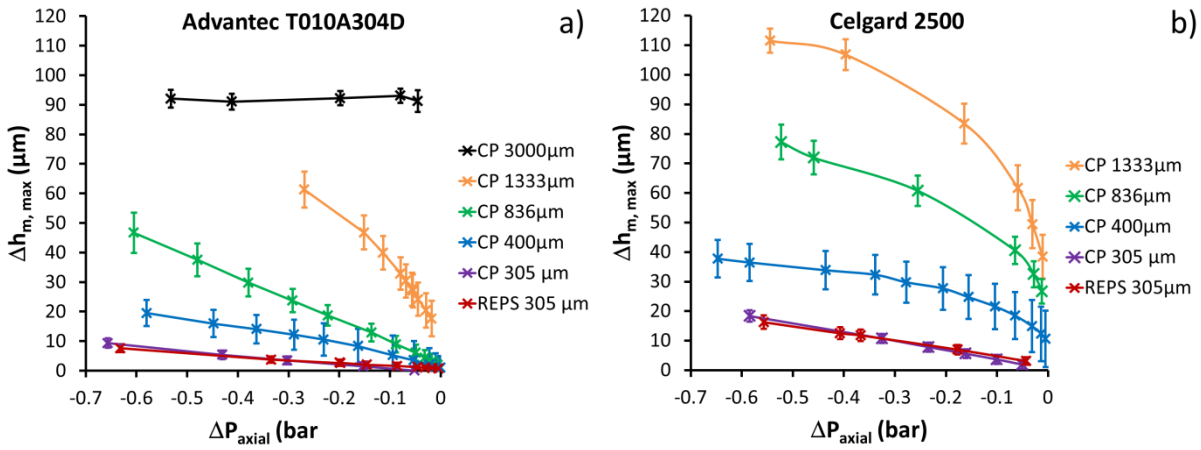

Fig. 9: $\Delta h_{m,\,max}$ in function of ΔP_{axial} for two different membranes: a) Advantec T010A304D: PTFE, δ = 70 µm, ε = 68%; b) Celgard 2500: PP, δ = 25 µm, ε = 55%.

3.3 Impact of the spacer design on the pressure drop

As seen in Fig. 7, the membrane deflection itself can influence the axial pressure drop considerably. However, decreasing the interpillar distance to decrease this membrane deflection can equally result in a negative impact on the axial pressure drop and consequently in a larger pressure difference across the membrane, potentially leading to breakthrough. To this end, ΔP_{axial} was measured in function of the flow rate for the different spacer designs using the set-up depicted in Fig. 6 (see supporting information §S.2 for the used procedure).

Looking at Fig. 10a-b, it is seen that $\Delta P_{m,\,max}$ decreased when the interpillar distance decreased from 3000 µm to 836 µm, which can be explained by a decreasing membrane deflection. At an interpillar distance of 836 µm the minimum value of 0.1 bar was even reached for both membranes. For the interpillar spacing of 3000 µm and 1333 µm, $\Delta P_{m,\,max}$ strongly increased with the flow rate, which was due to the fact that membrane deflection and the axial pressure drop intensify one another. At near complete membrane deflection the axial pressure drop is large, creating a high pressure difference across the membrane, which again increases membrane deflection and so on. This will quickly result in breakthrough. When the interpillar distance for CPs was decreased to below 836 µm, $\Delta P_{m,\,max}$ again increased because of the higher hydraulic resistance, due to the narrower gap between the pillars. However, if the REP spacer geometry with an interpillar spacing of 305 µm was used, $\Delta P_{m,\,max}$ again decreased to nearly 0.1 bar. This can be explained on the one hand by a higher porosity and more uniform interpillar spacing that is obtained with diamond shaped pillars than with circular shaped pillars. Hence, the REPs are positioned parallel to one another, creating a more uniform interpillar spacing throughout the channel (Fig. 8). On the other hand wedges were used with REPs. These wedges give a soft transition of the distributor features with an AR of 10 to the spacer features with an AR of 1, guaranteeing throughout the entire channel a constant interpillar spacing of 305 µm. With CPs, on the contrary, no wedges were present, creating a transition zone between the distributor and CPs where the interpillar spacing is locally larger. The membrane will locally deflect

between the distributor and the CPs, which locally reduces the channel height. Consequently, the use of wedges is recommended.

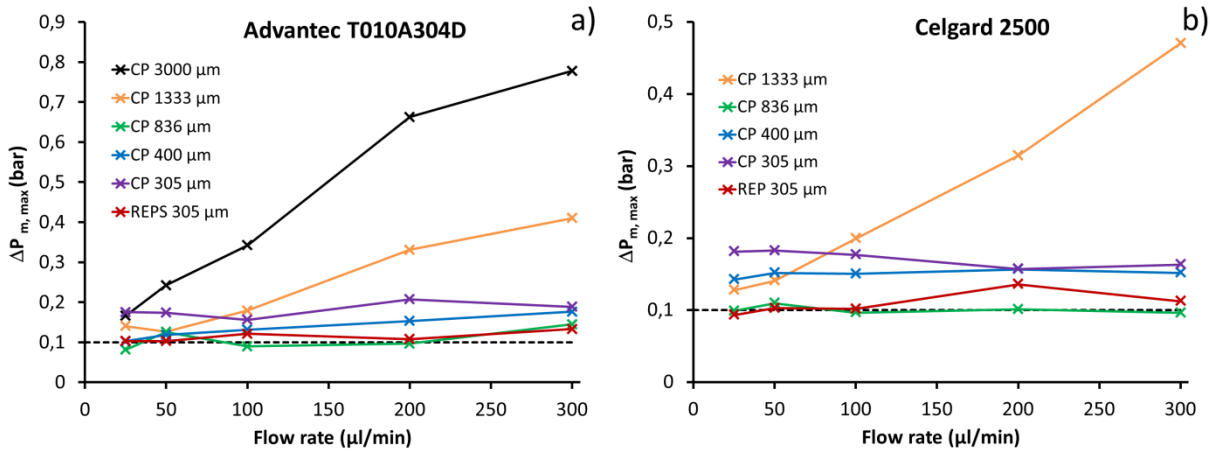

Fig. 10: $\Delta P_{m,\,max}$ in function of the flow rate for a) the Advantec T010A304D membrane and b) the Celgard 2500 membrane.

The pillar design can be optimized even further, by decreasing the size of the pillars itself. Doing so, the hydraulic resistance will decrease, as the porosity of the pillar array increases with decreasing pillar size. Moreover, also the internal volume of the MMC will increase with decreasing pillar size and therefore the throughput can be increased. However, when the pillars become smaller and smaller they also become more and more fragile and more difficult to fabricate because of the increased aspect ratio (width/depth). Consequently, the optimal pillar size is the smallest pillar that can be produced without fabrication errors with the used fabrication technique. This, however, falls beyond the scope of this work and has not been further investigated.

3.4 Impact of the membrane deflection on the mass transfer

The membrane deflection does not only influence $\Delta P_{m,\,max}$, but it will also affect the mass transfer. Depending on which phase wets the membrane (Fig. 2), two different global mass transfer coefficients can be derived [6] (Eqs. 1-2):

$$\frac{1}{K_f} = \frac{1}{k_f} + \frac{\delta\tau}{D_f\varepsilon} + \frac{1}{Hk_s} \quad (1)$$

$$\frac{1}{K_s} = \frac{1}{k_f} + \frac{\delta\tau}{D_s\varepsilon H} + \frac{1}{Hk_s} \quad (2)$$

where K_f is the global mass transfer coefficient when the pores are wetted by the feed solution, k_f the local mass transfer coefficient inside the feed channel, δ the membrane thickness, τ the membrane tortuosity, D_f the molecular diffusion coefficient of the solute in the feed phase, ε the membrane porosity, H the partition coefficient, k_s the mass transfer coefficient inside the solvent channel, K_s the global mass transfer coefficient when the pores are wetted by the solvent solution and D_s the molecular diffusion coefficient of the solute inside the solvent. The local mass transfer coefficients k_f and k_s can be calculated from the Sherwood number (Eq. 3) and depend on the channel height (h), which will alter when the membrane deflects (Fig. 2):

$$Sh = \frac{2\ k\ h}{D} \quad (3)$$

For a MMC channel with REPs as spacer features, spaced 305 µm apart, the Sherwood number is equal to 0.94 for both phases [9] and could be assumed constant [5]. At the operated flow rates the Graetz numbers (Gz < 6.2) are low, implying that the flow rate has a small to negligible influence on the Sherwood number [5]. When the membrane deflects, the height of both channels will be altered and consequently also the local and global mass transfer coefficient. In case the feed wets the membrane, the solvent always has a higher pressure than the feed to avoid breakthrough and because of this, the membrane can only deflect towards the feed channel. Depending on the partition coefficient and the diffusion coefficients of the solute in the feed and the solvent, this can have a positive or negative effect on K_f (Fig. 11a). A positive impact on K_f due to deflection of the membrane is observed when the slope of the curve is negative (Eq. 4):

$$\frac{d(K_f)}{dh_f} < 0 \; or \; \frac{d\left(\frac{1}{K_f}\right)}{dh_f} > 0 \tag{4}$$

Substituting Eqs. 1 and 3 into Eq. 4 yields Eq. 5:

$$\frac{D_f}{D_s} < H \tag{5}$$

From Eq. 5 it is seen that deflection of the membrane has a positive impact on the mass transfer as long as the ratio of the diffusion coefficients is smaller than the partition coefficient. This can be understood as follows. Assume that diffusion in the feed is twice as slow as in the solvent. As long as the partition coefficient is larger than 2 this has a positive impact on the mass transfer. Hence, the distance the solute has to diffuse in the feed channel, because of deflection of the membrane, is reduced, which in turns reduces the mass transfer resistance term of the feed channel (first term of Eq. 1). The mass transfer resistance term of the solvent channel (third term of Eq. 1) of course increases because of the larger distance the solute now has to diffuse. However, this increase is smaller than the decrease of the first term because of the larger diffusion coefficient of the solute in the solvent and/or the partition coefficient present in that term. The presence of the partition coefficient in this third term can be understood from the fact that the concentration gradient in the solvent channel is larger than in the feed channel and this result in a higher mass transfer in the solvent channel.

When $D_f/D_s > H$ the increase of the third mass transfer resistance term is no longer compensated by the decrease of the first term and deflection of the membrane has a negative impact on the mass transfer. As long as $D_f/D_s < H$, it can be concluded that in case of the feed wetting the pores it is better to have an as large as possible interpillar distance, at which breakthrough is still avoided.

When the solvent is inside the pores, the membrane can only deflect towards the solvent channel and the height of the feed channel can only increase. In a similar fashion the criteria for which deflection of the membrane is advantageous can be derived (Fig. 11b) (Eqs. 6-7):

$$\frac{d(K_s)}{dh_f} > 0 \; or \; \frac{d\left(\frac{1}{K_s}\right)}{dh_f} < 0 \tag{6}$$

$$\frac{D_f}{D_s} > H \tag{7}$$

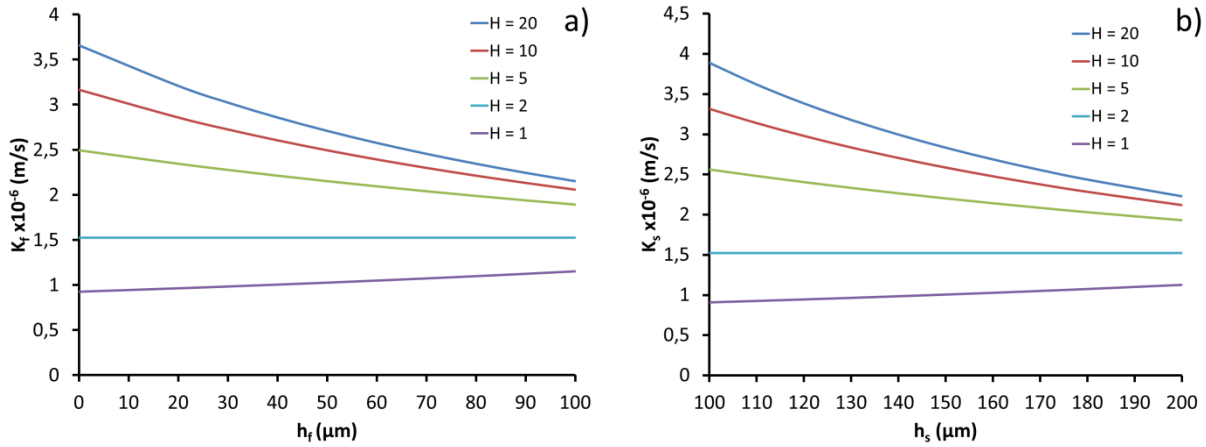

Fig. 11: a) K_f and b) K_s in function of the height of the feed channel for different partition coefficients with $D_f = 10^{-9}$ m²/s, $D_s = 0.5 \times 10^{-9}$ m²/s, $\delta = 20$ µm, $\tau = 4.5$, $\varepsilon = 0.39$, Sh = 0.94 and $h_f + h_s = 200$ µm.

Hence, when the solvent is inside the pores and as long as $D_f/D_s < H$, deflection of the membrane has a negative impact on the mass transfer. For most applications D_f/D_s is indeed smaller than the partition coefficient. In that case and with the solvent inside the pores, a narrow interpillar spacing (e.g. 305 µm) will yield the highest mass transfer. The effect of membrane deflection and the accompanying impact of K_s on the throughput of the MMC can be calculated from Eq. 8 for co-current flow [6] and is depicted in Fig. 12. Increasing h_f from 100 µm to 190 µm, reduces the maximum flow rate, at which 99% of the equilibrium is still obtained, from 40 µl/min to 24 µl/min for H = 20 and $D_f/D_s = 2$.

$$\frac{C_s}{C_f} = \frac{1 - e^{-\frac{KL}{u_f h_f}\left(1+\frac{\alpha_f}{\alpha_s}\right)}}{\frac{\alpha_f}{H\alpha_s} e^{-\frac{KL}{u_f h_f}\left(1+\frac{\alpha_f}{\alpha_s}\right)} + \frac{1}{H}} \tag{8}$$

$$\alpha_f = \frac{u_f h_f}{KL} \qquad \alpha_s = \frac{u_f h_f H}{KL} \tag{9}$$

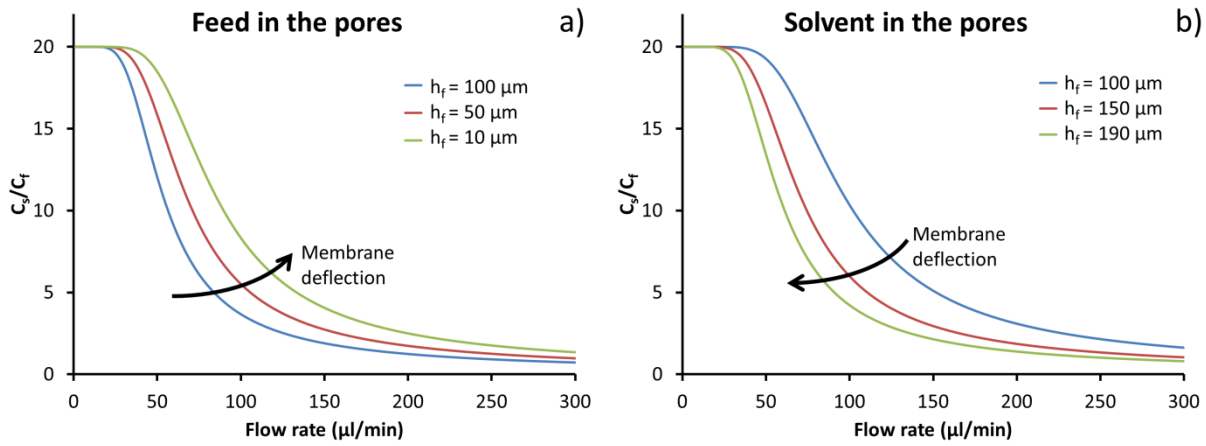

Fig. 12: C_s/C_f as function of the flow rate for different deflection heights in cocurrent mode with a flow rate ratio of 1: a) with feed and b) with solvent inside the pores of the membrane. H = 20, D_f = 1 x 10^{-9} m²/s, D_s = 0.5 x 10^{-9} m²/s, δ = 20 µm, τ = 4.5, ε = 0.39, Sh = 0.94, L = 99 mm, w = 13 mm and $h_f + h_s$ = 200 µm.

When the solvent is inside the pores and the partition coefficient is larger than one, the membrane resistance term will be lower than when the feed is inside the pores, due to the appearance of the partition coefficient in the membrane resistance term [6], [10]. Membranes with the solvent inside the pores will therefore generally lead to faster extraction kinetics. This is true in absence of membrane deflection (e.g. hollow fibers). However, when deflection is taken into account, this is no longer unconditionally valid. If $D_f/D_s < H$, K_f is the largest under following condition (Eq. 10):

$$\lim_{h_f \to 0} \frac{1}{K_f} = \frac{\delta\tau}{D_f \varepsilon} + \frac{1}{Hk_s} \tag{10}$$

In that case h_s is also equal to h_{tot} ($h_{tot} = h_s + h_f$). K_s is maximal when there is no deflection of the membrane. In this case, solvent inside the pores is then only favorable under following condition (Eq. 11):

$$\left(\lim_{h_f \to 0} \frac{1}{K_f}\right) > \left(\frac{1}{K_s}\right)_{h_f = h_s = h_0} \tag{11}$$

Substituting Eqs. 2, 3 and 10 into Eq. 11 yields Eq. 12:

$$\frac{\delta_f \tau_f}{D_f \varepsilon_f} + \frac{2\, h_{tot}}{Sh\, H\, D_s} > \frac{2h_0}{Sh\, D_f} + \frac{\delta_s \tau_s}{D_s \varepsilon_s H} + \frac{2h_0}{Sh\, D_s H} \tag{12}$$

Rearranging Eq. 12 yields Eq. 13:

$$1 > \frac{2h_0 \left(HD_s - D_f\right)\varepsilon_f}{Sh\, D_s H \delta_f \tau_f} + \frac{\delta_s \tau_s \varepsilon_f D_f}{\delta_f \tau_f \varepsilon_s D_s H} \tag{13}$$

Using Eq. 13, under the condition that $D_f/D_s < H$, allows to determine which spacer structure yields the highest mass transfer coefficient in case a hydrophilic and hydrophobic membrane is at one's disposal. Hence, only when the right term of Eq. 13 is smaller than 1, the membrane in which the solvent is inside the pores along with a small interpillar spacing (e.g. 305 µm) to prevent membrane deflection, will yield the highest mass transfer. When this term is larger than 1, membrane deflection has a positive impact on the mass transfer with a membrane in which the feed is inside the pores. Hence, mass transfer will then be the highest with a spacer with interpillar spacing as large as possible without provoking breakthrough. Depending on the outcome of Eq. 13, membrane deflection can thus have either a negative or positive impact on the mass transfer.

4 Conclusions

The impact of the spacer features (interpillar distance and shape) on membrane deflection, pressure difference across the membrane, and mass transfer was studied. It can be concluded that the smaller the interpillar distance became, the smaller the membrane deflection was. However, this was not the case for the pressure difference across the membrane. Decreasing the interpillar distance for the CP from 3000 µm to 836 µm, lowered the pressure difference across the membrane. However, further reduction of the interpillar distance again increased the pressure difference across the membrane, because of a higher hydraulic resistance, due to a smaller gap between the pillars. Using a REP design with wedges, uniform interpillar spacing could be guaranteed, reducing the pressure difference across the membrane to 0.1 bar, which was the minimal set-point. Using REPs the membrane deflection was smaller than 10 µm up to an axial pressure drop of 0.35 bar. Subsequently, design rules could be provided, which allows for choosing the best spacer design to maximize mass transfer. Interestingly, the membrane deflection can have either a positive or negative impact on the mass transfer.

5 Acknowledgements

W. De Malsche greatly acknowledges the Flemish Fund for Scientific Research (FWO) for support through a Post-Doctoral grant (81409). J. Hereijgers (111140) is supported through a specialization grant from the Instituut voor Wetenschap en Technologie (IWT) from the Flanders region. This work was supported in part by the OZR of the Vrije Universiteit Brussel through the Strategic Research Program (SRP-Groeier) entitled ‘Polymer microfluidic devices for integrated (bio-)chemical separation and detection’.

The authors have declared no conflict of interest.

6. References

[1] G. M. Ritcey and A. W. Ashbrook, *Solvent extraction: principles and applications to process metallurgy - Volume I*. Amsterdam: Elsevier, 1984.

[2] E. Drioli, A. Criscuoli, and E. Curcio, *Membrane Contactors: Fundamentals, Applications and Potentialities*. Amsterdam: Elsevier, 2005.

[3] S. P. Nunes and K.-V. Peinemann, *Membrane Technology in the Chemical Industry*. Wiley-VCH, 2006.

[4] Z. F. Cui and H. S. Muralidhara, *Membrane Technology - A Practical Guide to Membrane Technology and Applications in Food and Bioprocessing*. Elsevier Ltd, 2010.

[5] J. Hereijgers, T. Vandermeersch, N. Van Oeteren, H. Verelst, H. Song, D. Cabooter, T. Breugelmans, and W. De Malsche, "Separation of Co(II)/Ni(II) with Cyanex 272 using a flat membrane microcontactor: Extraction kinetics study," *J. Memb. Sci.*, vol. 499, pp. 370–378, Oct. 2015.

[6] J. Hereijgers, M. Callewaert, X. Lin, H. Verelst, T. Breugelmans, H. Ottevaere, G. Desmet, and W. De Malsche, "A high aspect ratio membrane reactor for liquid-liquid extraction," *J. Memb. Sci.*, vol. 436, pp. 154–162, Feb. 2013.

[7] J. Hereijgers, T. Breugelmans, and W. De Malsche, "Breakthrough in a flat channel membrane microcontactor," *Chem. Eng. Res. Des.*, vol. 94, pp. 98–104, 2015.

[8] J. Billen, P. Gzil, N. Vervoort, G. V. Baron, and G. Desmet, "Influence of the packing heterogeneity on the performance of liquid chromatography supports," *J. Chromatogr. A*, vol. 1073, no. 1–2, pp. 53–61, May 2005.

[9] J. Hereijgers, N. van Oeteren, J. F. M. Denayer, T. Breugelmans, and W. De Malsche, "Multistage counter-current solvent extraction in a flat membrane microcontactor," *Chem. Eng. J.*, vol. 273, pp. 138–146, 2015.

[10] N. A. D'Elia, L. Dahuron, and E. L. Cussler, "Liquid-liquid extractions with microporous hollow fibers," *J. Memb. Sci.*, vol. 29, no. 3, pp. 309–319, Dec. 1986.